Low-Temperature Magnetic Properties of Hematite Nanorods

Yimin Zhao,[†] Charles W. Dunnill,[‡] Yanqiu Zhu,*[,†] Duncan H. Gregory,*[,‡] Walter Kockenberger,[§] Yanhui Li,[†] Weibing Hu,[†] Iftikhar Ahmad,[†] and David G. McCartney[†]

The Schools of Mechanical, Materials and Manufacturing Engineering and of Physics and Astronomy, University of Nottingham, University Park, Nottingham NG7 2RD, and WestCHEM, Department of Chemistry, Joseph Black Building, University of Glasgow, Glasgow G12 8QQ, United Kingdom

Received October 5, 2006. Revised Manuscript Received December 14, 2006

Low-temperature magnetic properties of hematite nanorods, prepared by both iron−water vapor reactions (sample 1) and hydrothermal methods (sample 2), were studied by superconducting quantum interference device (SQUID) magnetometry. The Morin transition temperature was found to be 122 K in hematite nanorod sample 1, and an unexpected phenomenon was found under an applied field of 10 Oe. These nanorods (sample 1) show an abrupt *decrease* of the magnetic susceptibility at ca. 122 K, contrary to the abrupt *increase* normally attributed to the Morin transition in bulk hematite. The origin of this phenomenon can be traced to the probable coherence of the one-dimensional shape anisotropy with the magnetocrystalline anisotropy. In contrast, no obvious Morin transition was found in hematite nanorod sample 2.

Introduction

The magnetic properties of hematite (hexagonal or rhombohedral α-Fe_2O_3) in bulk form and as spherical nanoparticles have been intensively studied because they have various applications in magnetic storage devices, spin electronics devices, drug delivery, tissue repair engineering, and magnetic resonance imaging.[1−7] In contrast to spherical nanoparticles, nanorods with their inherent one-dimensional (1-D) shape anisotropy may exhibit unique magnetic behavior which is significantly different from that of the bulk material.[8,9] However, few investigations of the magnetic properties of hematite nanorods have been reported. It is generally accepted that for bulk hematite the shape anisotropy is not important due to the low saturation magnetization ($\mathbf{M}_S$) since the shape anisotropy field is proportional to $\mathbf{M}_S$. For 1-D nanorods with a high aspect ratio, the shape anisotropy may play an important role in dictating the magnetic properties. The magnetic domain structures, which determine the magnetic properties of the materials, have been reported to be affected by the 1-D nanostructure.[10−12] Furthermore, whereas the surface is not a significant consideration for bulk hematite, it will certainly constitute a large portion of a particle on the nanometer scale. The absence of three-dimensional (3-D) symmetry at the surface will change the magnetic spin orientations and therefore likely alter the magnetic properties, as is often observed in thin films.[13,14] Adatoms and nanoclusters adsorbed at the nanorod surfaces may also have an impact on the magnetic properties. Further, the impurities, defects, and internal stresses of the nanorods that are likely to strongly depend on the preparation methods could also be important factors influencing the magnetic properties.[7,15,16]

Below the Neél temperature ($T_N = 955$ K), bulk hematite is a canted weak ferromagnetic (WF) phase resulting from the nonexact compensation of the two magnetic sublattices with spins lying in the basal plane {rhombohedral (111)}. The oxide transforms to an antiferromagnetic (AF) phase with the two antiparallel magnetic sublattices lying along the *c* axis {rhombohedral [111]} below 260 K (Morin transition temperature, T_M).[17] It has been reported that the particle shape, size, crystallinity, and surface will affect the value of T_M.[3,18−21] T_M tends to decrease with particle size

* To whom correspondence should be addressed. E-mail: yanqiu.zhu@nottingham.ac.uk (Y.Z.); d.gregory@chem.gla.ac.uk (D.H.G.).
† The School of Mechanical, Materials and Manufacturing Engineering, University of Nottingham.
‡ University of Glasgow.
§ The School of Physics and Astronomy, University of Nottingham.

(1) Bodker, F.; Hansen, M. F.; Koch, C. B.; Lefmann, K.; Morup, S. *Phys. Rev. B* **2000**, *61*, 6826−6838.
(2) Zysler, R. D.; Fiorani, D.; Testa, A. M.; Suber, L.; Agostinelli, E.; Godinho, M. *Phys. Rev. B* **2003**, *68*, 212408−21241.1.
(3) Zysler, R. D.; Fiorani, D.; Testa, A. M.; Godinho, M.; Agostinelli, E.; Suber, L. *J. Magn. Magn. Mater.* **2004**, *272*, 1575−1576.
(4) Murphy, C. J.; Jana, N. R. *Adv. Mater.* **2002**, *14*, 80−82.
(5) Cordente, N.; Respaud, M.; Senocq, F.; Casanove, M. J.; Amiens, C.; Chaudret, B. *Nano Lett.* **2001**, *10*, 565−568.
(6) Gupta, A. K.; Gupta, M. *Biomaterials* **2005**, *26*, 3995−4021.
(7) Rath, C.; Sahu, K. K.; Kulkarmi, S. D.; Anand, S.; Date, S. K.; Das, R. P.; Mishra, N. C. *Appl. Phys. Lett.* **1999**, *75*, 4171−4173.
(8) Gregg, K. A.; Perera, S. C.; Lawes, G.; Shinozaki, S.; Brock, S. L. *Chem. Mater.* **2006**, *18*, 879−886.
(9) Kumar, A.; Fahler, S.; Schlorb, H.; Leistner, K.; Schultz, L. *Phys. Rev. B* **2006**, *73*, 064421−064425.
(10) Henry, Y.; Ounadjela, K.; Piraux, L.; Dubois, S.; George, J. M.; Duvail, J. L. *Eur. Phys. J. B* **2000**, *20*, 35.
(11) Watanabe, K.; Takemura, Y.; Shimazu, Y.; Shirakashi, J. *Nanotechnology* **2004**, *15*, S566−S569.
(12) Thiaville, A.; Garcia, J. M.; Miltat, J. *J. Magn. Magn. Mater.* **2002**, *242*, 1061−1063.
(13) Kittle, C. *Phys. Rev.* **1946**, *70*, 965−971.
(14) Peacock, R. V.; Winsor, G. *Nature* **1962**, *193*, 768.
(15) Raming, T. P.; Winnubst, A. J. A.; Van Kats, C. M.; Philipse, A. P. *J. Colloid Interface Sci.* **2002**, *249*, 346−350.
(16) Fiorani, D.; Testa, A. M.; Suber, L.; Angiolini, M.; Montone, A.; Polichetti, M. *Nanostruct. Mater.* **1999**, *12*, 939−942.
(17) Morin, F. J. *Phys. Rev.* **1950**, *78*, 819−820.
(18) Mansilla, M. V.; Zysler, R. D.; Arciprete, C.; Dimitrijewits, M.; Sierra, D. R.; Saragovi, C. *J. Magn. Magn. Mater.* **2001**, *226*, 1907−1909.
(19) Amin, N.; Arajs, S. *Phys. Rev. B* **1987**, *35*, 4810−4811.

10.1021/cm062375a CCC: $37.00
Published on Web 01/23/2007

and almost vanish for a spherical particle with a diameter of less than 10 nm. Doping of impurities, vacancies, strains, and crystal defects also reduce T_M. There are only sporadic experimental data concerning the value of T_M for hematite nanorods (or nanowires), with a general consensus that T_M is much lower than that for the bulk oxide. Acicular hematite nanorods (70 nm in diameter and 330 nm long) have a T_M of 170 K,[16] nanowires with a diameter of 120 nm have a T_M of 80 K,[22] and rods with a diameter of 20 nm did not show a transition down to 4 K.[23] Sorescu and co-workers have studied different hematite particles with polyhedral, platelike, disk-shaped, and needlelike morphology, prepared by hydrothermal methods, using Mössbauer spectroscopy.[24] Their results have shown that the WF and AF phases coexist below T_M, but the population of WF phases strongly depends on the morphology. Among all of the different morphologies in their studies, needlelike hematite particles have the largest WF phase fraction (>50 wt % below 150 K). No explanations for this phenomenon were forthcoming. Most recently, the Morin transition has been found to be completely suppressed in mesoporous hematite and hematite nanotubes due to a long-range magnetic ordering.[25,26] Overall, the magnetic behavior and spin reorientation of hematite nanorods at low temperatures around T_M are still not fully understood, and this area requires further study. In this work, using SQUID magnetometry, we have studied the low-temperature magnetic properties of two types of hematite nanorods prepared first by iron−water vapor reactions and second by hydrothermal methods.

Experimental Section

Hematite nanorods were prepared by an iron−water reaction (sample 1) and by a hydrothermal technique (sample 2). Sample 1 was synthesized via a simple iron−water reaction method that we have reported elsewhere.[27] In brief, water vapor was introduced to the reaction tube in a stream of Ar carrier gas to react with the micrometer-sized iron particles at an optimum condition of 350 °C for 4 h. The resulting needlelike hematite nanorods can be physically separated from the iron particles by ultrasonication. Sample 2, consisting of high-quality, single-crystalline hematite nanorods, was prepared using a hydrothermal technique similar to that reported recently for hematite nanotube production.[28] A mixture of $FeCl_3$ (0.2 mL, Sigma-Aldrich, 45% solution, pure) and $NH_4H_2PO_4$ (3 mg, Sigma-Aldrich, 99.999%) in 40 mL of water was sealed in a stainless steel pressure vessel and heated at 200 °C for 2 h. The precipitate was centrifuged and washed with deionized water several times to remove the residual salt byproducts. The morphology and microstructure of the samples were characterized by transmission electron microscopy (TEM; Jeol-2000FX, operated at 200 kV) and electron diffraction (ED). Infrared spectra were recorded using a Perkin-Elmer 2000-FTIR spectrometer using a KBr-supported sample wafer in a Pyrex vacuum IR cell. The magnetic susceptibility of the samples was measured using a Quantum Design MPMS-XL 5T SQUID magnetometer. All samples were loaded in a nitrogen-filled recirculating glovebox. Data were collected between 2 and 200 K under applied fields of 100 and 10 Oe with points at 1 K intervals between 2 and 30 and 5 K intervals from 30 to 200 K under FC and ZFC conditions. Field-dependent measurements were made under applied fields of $-5 \times 10^4 \leq \mathbf{H}/\mathrm{Oe} \leq 5 \times 10^4$ at 200 K. Data were corrected for core diamagnetism and the diamagnetic contribution of the sample holders (gelatin capsules).

Results and Discussion

Morphology and Microstructure. The morphology and microstructure of samples 1 and 2 are presented in Figure 1. The needlelike hematite nanorods obtained after separation of iron particles by sonication (sample 1**)** are shown in Figure 1a and are typically around 1.5−2 μm in length with an average diameter from 20 nm (tip) to 100 nm (base). Figure 1a also shows that most of the nanorods attain a length of more than 1 μm. As discussed in refs 27 and 28, sample 1 may contain a minute amount of magnetite and sample 2 is pure hematite. The ED pattern in Figure 1b indicates that the nanorods are single crystalline. The acicular nanorods of sample 2 are shown in Figure 1c,d and exhibit a much more uniform shape and size compared to those of sample 1. The ellipsoidal nanorods have a long axis of ca. 400−450 nm and a short axis of ca. 50−60 nm. Figure 1d shows that the oval-shaped nanorods appear to have a rough surface and possibly some pores in the body. ED patterns reveal, as for sample 1, that the nanorods are also single crystalline. FTIR spectra of samples 1 and 2 are shown in Figure 2, in which the bands below 600 cm^{-1} were assigned to the Fe−O vibration mode of Fe_2O_3. The FTIR results suggest that there are no other species on the surface of the nanorods in sample 1 except for a weak peak at 1190 cm^{-1} which is related to C−OH stretching since we used ethanol to treat the sample. For sample 2, the presence of the band at 1630 cm^{-1} was attributed to C═C vibrations and that at 3430 cm^{-1} to the existence of large amounts of residual hydroxyl groups. The presence of the bands at around 900−1000 cm^{-1} in sample 2 (Figure 2b) is indicative of the adsorption of phosphate on the nanorod surface. This result is similar to that observed for hematite nanotubes prepared using the same precursors,[28] and the adsorbed phosphate ions cannot be removed by simple washing. It is noteworthy that the bands related to the Fe−O vibration in sample 2 are shifted and much weaker than those related to the Fe−O vibration in sample 1, which may be attributed to the smaller particle size, porosity within the body of the nanorods (Figure 1d), and ion adsorption on the surface. In a previous report,[29] it had been shown that

(20) Kundig, W.; Bommel, H.; Constabaris, G.; Lindquist, R. H. *Phys. Rev.* **1966**, *142*, 327−333.
(21) Schroeer, D.; Nininger, R. C., Jr. *Phys. Rev. Lett.* **1967**, *19*, 632−634.
(22) Xue, D. S.; Gao, C. X.; Liu, Q. F.; Zhang, L. Y. *J. Phys.: Condens. Matter* **2003**, *15*, 1455−1459.
(23) Xu, Y. Y.; Rui, X. F.; Fu, Y. Y.; Zhang, H. *Chem. Phys. Lett.* **2005**, *410*, 36−38.
(24) Sorescu, M.; Brand, R. A.; Tarabassanu, D. M.; Diamandescu, L. *J. Appl. Phys.* **1999**, *85*, 5546−5548.
(25) Jiao, F.; Harrison, A.; Jumas, J. C.; Chadwick, A. V.; Kockelmann, W.; Bruce, P. G. *J. Am. Chem. Soc.* **2006**, *128*, 5468−5474.
(26) Liu, L.; Kou, H. Z.; Mo, W. L.; Liu, H. J.; Wang, Y. Q. *J. Phys. Chem. B* **2006**, *110*, 15218−15223.
(27) Zhao, Y. M.; Li, Y. H.; Ma, R. Z.; Roe, M. J.; McCartney, D. G.; Zhu, Y. Q. *Small* **2006**, *2*, 422−427.
(28) Jia, C. J.; Sun, L. D.; Yan, Z. G.; You, L. P.; Luo, F.; Han, X. D.; Pang, Y. C.; Zhang, Z.; Yan, C. H. *Angew. Chem., Int. Ed.* **2005**, *44*, 4328−4333.
(29) Cornell, R. M.; Schwertmann, U. *The Iron Oxides: structure, properties, reactions, occurrences and uses*; Wiley-VCH Verlag GmbH & Co. KgaA: Weinheim, Germany, 2003; p 141.

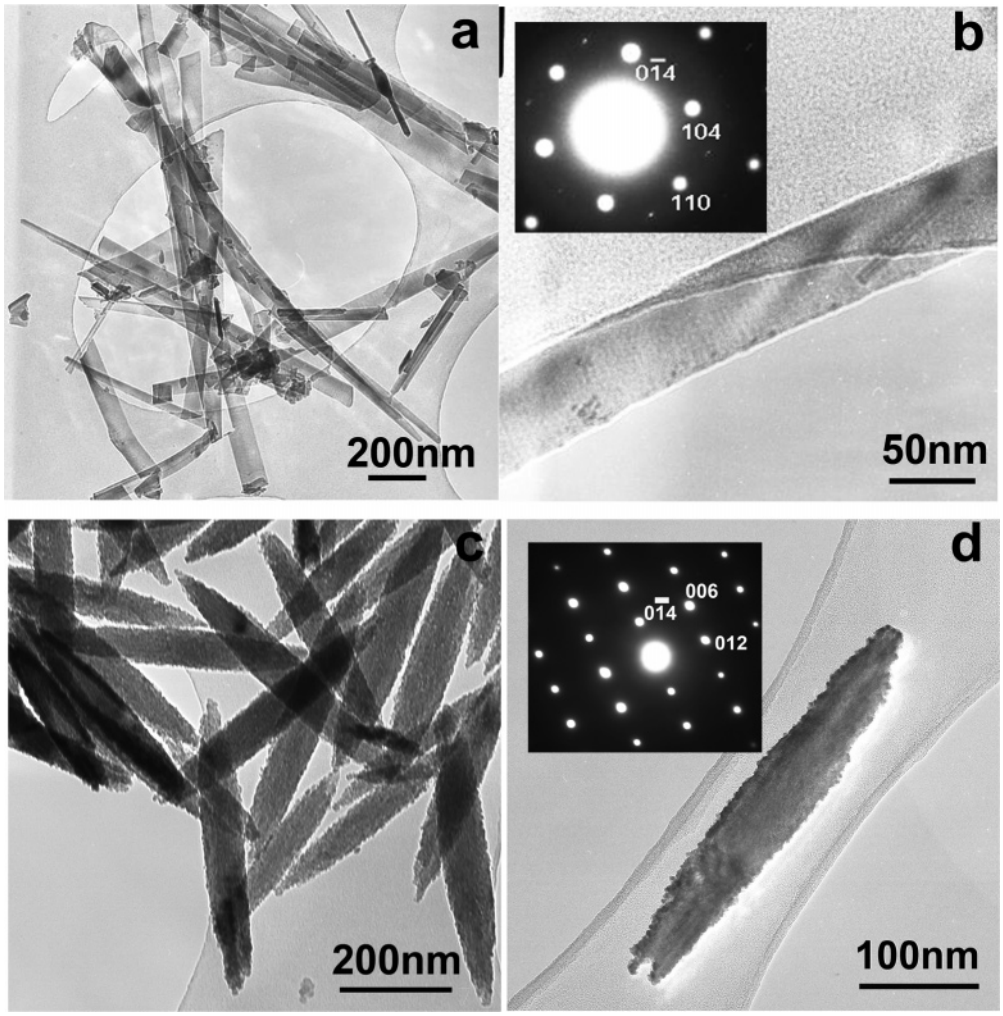

Figure 1. TEM images of the hematite nanorods: (a, b) sample 1 prepared by the iron−water reaction (the inset ED pattern has a zone axis of [$4\bar{4}1$]), (c, d) sample 2 prepared by the hydrothermal technique and the ED pattern with zone axis [100].

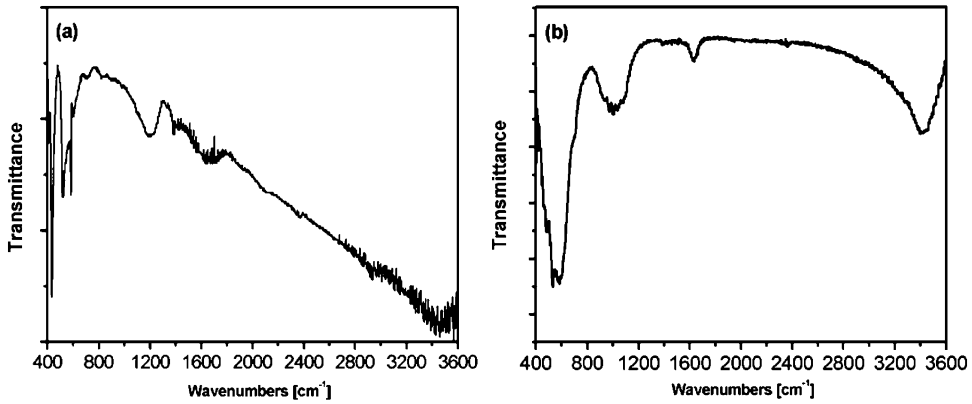

Figure 2. FTIR spectra of hematite nanorods: (a) sample 1 prepared by the iron−water reaction, (b) sample **2** prepared by hydrothermal methods.

IR peaks of iron oxides are sensitive to the particle size, shape, degree of crystallinity, and ions which are bonded to the surface.

Magnetic Properties. Parts a and b, respectively, of Figure 3 show the magnetic susceptibility versus temperature relationship and the hysteresis loop at 200 K for sample 1; the susceptibility versus temperature behavior and the hysteresis loop at 200 K for sample 2 are shown in parts c and d, respectively, of Figure 3. The two types of nanorods exhibit significantly different magnetic behaviors.

First, the hysteresis loops of the two samples indicate different magnetic domain type behavior. On the basis of the criteria given by Dunlop,[29] single-domain (SD) particles have a value of $\mathbf{M}_R/\mathbf{M}_S$ (where $\mathbf{M}_R$ is the remanence and $\mathbf{M}_S$ is the saturation magnetization) larger than 0.5, pseudo-single-domain (PSD) particles have a value between 0.1 and

(30) Dunlop, D. J. *Rep. Prog. Phys*. **1990**, *53*, 707−792.

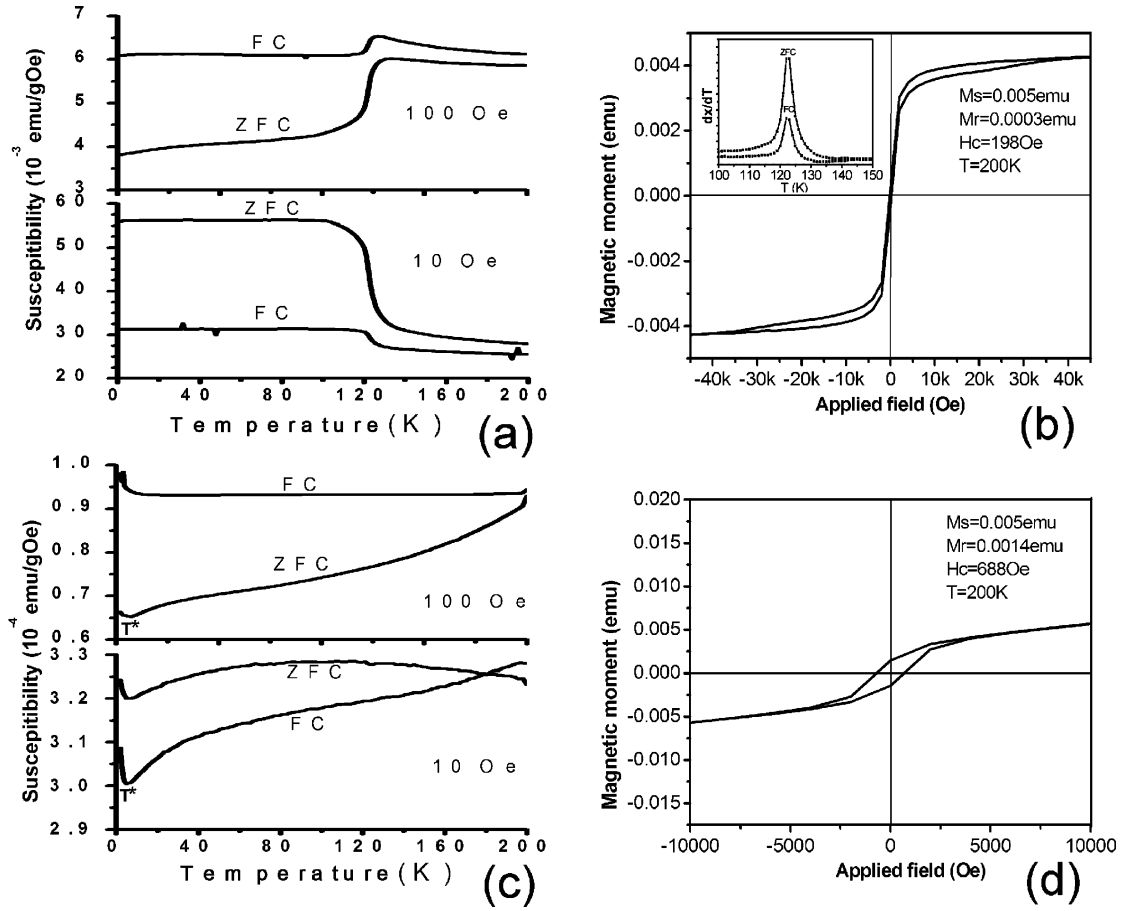

Figure 3. Magnetic susceptibility temperature dependence and hysteresis loops of hematite nanorods: (a, b) sample 1 prepared by iron−water vapor reactions, (c, d) sample 2 prepared by hydrothermal techniques. The inset in (b) is the dχ/dT versus T curve for sample 1 when an external field of 100 Oe was applied.

0.5 and multidomain (MD) particles have a value lower than 0.1. From Figure 3b,d, it is noted that the hematite nanorods in sample 1 show an MD-type behavior ($\mathbf{M}_R/\mathbf{M}_S = 0.06$), whereas those in sample 2 show a PSD-type behavior ($\mathbf{M}_R/\mathbf{M}_S = 0.28$).

Second, the magnetic susceptibility of sample 1 is about 2 orders of magnitude larger than that of sample 2. In terms of the magnetic domain type, to change the magnetization of an MD particle, the domain wall must be translated, which is an energetically easy process. However, to change the magnetization of an SD particle, it is necessary to rotate the entire magnetization, which is an energetically difficult process. Therefore, MD particles often have a larger magnetic susceptibility and a lower coercive field than SD particles. As can be seen in Figure 3a,c, the hematite nanorods in sample 1 have a much larger susceptibility than those in sample 2; further parts b and d of Figure 3 illustrate that the nanorods in sample 1 exhibit a lower coercive field (198 Oe) than those in sample 2 (688 Oe).

Last, an abnormal phenomenon was observed in nanorods of sample 1. As shown in Figure 3a, under an external field of 100 Oe, an abrupt susceptibility increase occurs at 122 K, indicative of the hematite's Morin transition from the AF phase to the WF phase. T_M was determined by the sharp peak in the dχ/dT versus T curve, as shown in the inset in Figure 3b. Interestingly, under an external field of 10 Oe, an abrupt susceptibility *decrease* takes place at a similar temperature, i.e., T_M. This phenomenon is unlikely to arise, for example, from the minute amount of magnetite impurities in the sample because magnetite does not exhibit such a spin flip behavior. By contrast again, sample 2 shows only weak curvature in the zero-field-cooling (ZFC) curves and no apparent Morin transition (Figure 3c).

Discussion

For conventional bulk materials, as the grain size decreases to a critical value the particle will change from MD type to SD type. For hematite, the critical size for an MD to SD conversion is usually very large (>15 μm) due to the low saturation magnetization $\mathbf{M}_S$.[31] However, our results appear to suggest that the hematite nanorods in sample 1, having a diameter between 20 and 100 nm and a length of less than 2 μm, possess MD behavior. With regard to the abrupt decrease of the susceptibility of sample 1 at ca. 120 K under a field of 10 Oe, the result contrasts with the generally observed increase at T_M, corresponding to the transition from the AF to the WF phase. This phenomenon seen in sample 1, to the best of our knowledge, has never been reported for bulk hematite or spherical nanoparticles, and no such transition is observed for sample 2.

Magnetic anisotropy is considered to be one of the key factors controlling the properties of magnetic nanorods.

(31) Kletetschka, G.; Wasilewski, P. J. *Phys. Earth Planet. Inter.* **2002**, *129*, 173−179.

Magnetocrystalline anisotropy will favor the magnetization along a preferred crystal orientation. In a textured nanorod, the shape anisotropy may compete with the magnetocrystalline anisotropy. For bulk hematite, the magnetocrystalline anisotropy field can be described as

$$\mathbf{H}_{K_1} = -K_1(\cos^2\theta_1 + \cos^2\theta_2)/2^{32} \quad (1)$$

where K_1 is the anisotropy energy constant and θ_1 and θ_2 are the angles of the two magnetization sublattices subtended with the *c*-axis (rhombohedral [111]) of hematite. A change in sign of K_1 then accounts for the Morin transition. When $T > T_M$ and $K < 0$, the atomic magnetic moments will lie in the basal plane to reduce the energy caused by the magnetocrystalline anisotropy, while, when $T < T_M$ and $K_1 > 0$, the atomic magnetic moments lie along the *c* axis. The maximum magnetocrystalline anisotropy field $\mathbf{H}_{K_1}$ has been determined to be 11.8 Oe on the basis of reported experimental data.[31] For an isolated nanorod, the shape anisotropy field can be described as

$$\mathbf{H}_{A,shape} = \mathbf{M}_S \times \Delta\mathbf{N}^9 \quad (2)$$

where $\mathbf{M}_S$ is the saturation magnetization (2.1 emu/cm^3 for bulk hematite)[32] and $\Delta\mathbf{N}$ is the demagnetization difference between the long axis and short axis of the nanorod. $\Delta\mathbf{N}$ increases as the aspect ratio of a nanorod increases. Using the values calculated by Bozorth,[33] a nanorod with an aspect ratio >10, as is the case in sample 1, can be viewed as infinite and gives a value of 0.5 for $\Delta\mathbf{N}$. The shape anisotropy field $\mathbf{H}_{A,shape} = 0.5 \times 2.1$ emu/cm^3 $= 1.05$ emu/cm^3 $= 13.2$ Oe. As for the hematite nanorods in sample 2, the aspect ratio of 8−9 leads to a value of 0.48 for $\Delta\mathbf{N}$ and $\mathbf{H}_{A\ shape} = 0.48 \times 2.1$ emu/cm^3 $= 1.00$ emu/cm^3 $=12.7$ Oe. The shape anisotropy energy will tend to favor the magnetization along the long axis of the nanorods. Since the shape anisotropy energy is comparable to the magnetocrystalline anisotropy energy, they will compete with each other, and the resulting magnetization will lie in a direction to minimize the total energy. The contribution of the shape anisotropy energy and the surface energy in nanorods becomes more important than that in bulk hematite; therefore, the normal macroscopic magnetization characteristics of the hematite may be altered significantly. In a special case, such as when the long axis of the nanorods is coexistent with the magnetocrystalline direction, the magnetization will lie along the long axis. For the case of a ferromagnetic nanorod with large $\mathbf{M}_S$, if the shape anisotropy energy is much larger than the magnetocrystalline anisotropy energy, the magnetization will also lie along the long axis of the nanorods, as reported in many works.[10−12,34] From the TEM images and the ED patterns in Figure 1, we know that the nanorods in sample **2** grow along the *c* direction; therefore, below $T_\mathbf{M}$ the magnetization will lie along the long axis of the nanorods. However, nanorods in sample 1 (growth direction [118]) grow neither along the *c* axis nor along a direction in the basal plane, and thus, below T_M the magnetization lies in a resultant direction arising from the coherence of the shape anisotropy and the magnetocrystalline anisotropy. Above T_M, there are three possible preferred axes each separated by 60° in a basal plane. Taking into account the shape anisotropy, we can deduce that the magnetic moment may lie in the axis that forms the smallest angle with the long axis of the nanorods to reduce the demagnetization field. Meanwhile, due to the competition of the magneticcrystalline anisotropy and the shape anisotropy, the critical size for SD in the hematite nanorods should also be different from that of 15 μm obtained for the bulk form. In sample 1, with a length of typically only 1−2 μm, we observed an MD-type behavior. The most often observed head−head domain structure in nanorods,[10−12] in which the magnetic moments lie along the easy axis in the basal plane forming the smallest angle with the long axis of a nanorod (Figure 4a), may explain the MD formation in the hematite nanorods. With reduced lengths for the nanorods in sample 2 (typically <500 nm) there may be only one or two domains; thus, the short nanorods exhibit PSD behavior (Figure 4b).

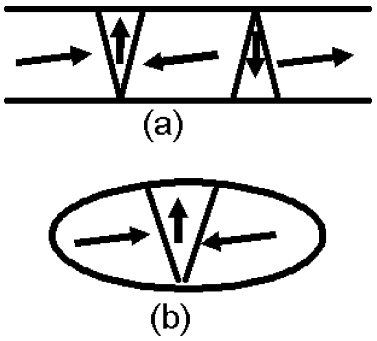

Figure 4. Proposed magnetic domain structure of the hematite nanorods: (a) MD in sample 1, (b) PSD in sample 2.

When a low external field of 10 Oe is applied, the effect of the shape anisotropy field (12−13 Oe, as described above) still plays an important role in determining the magnetization of the nanorods. Below T_M, the magnetocrystalline anisotropy tends to align the magnetization along the rhombohedral [111] axis and the shape anisotropy tends to align it along the long axis of the nanorods. Above T_M, magnetocrystalline anisotropy tends to align the magnetization in the basal plane while the shape anisotropy still tends to align it along the long axis of the nanorods. The competition of these two factors will align the magnetization along a certain direction to reach an overall minimum total energy. There will be a spin reorientation at the Morin transition. The "pinning" of the shape anisotropy may account for the sudden decrease in the susceptibility when the temperature reaches T_M, as shown in Figure 3a, under a small field of 10 Oe. This indicates that, when $T < T_M$, the magnetic susceptibility along the resultant direction has a larger value than that when $T > T_M$. However, when a large field is applied, it can overcome the pinning of the shape anisotropy, and the hematite nanorods will then exhibit the normal magnetic behavior at the Morin transition, as shown in Figure 3a under a field of 100 Oe.

(32) Morrish, A. H. *Canted Antiferromagnetism: Hematite*; World Scientific: Singapore, 1994; pp 27−53.
(33) Bozorth, R. N. *Ferromagnetism*; Wiley-IEEE: New York, 1993; p 849.
(34) Qin, D. H.; Lu, M.; Li, H. L. *Chem. Phys. Lett.* **2001**, *350*, 51−56.

We found that the T_M (122 K) of the hematite nanorods in sample 1 is much lower than the value of 260 K found for bulk hematite. T_M has been reported to decrease with a reduction in particle size.[3] Almost no Morin transition has been found for particles with a diameter less than 20 nm within the reported temperature range (usually higher than 4 K), although most authors claim that T_M should be even lower than the temperature limit used in their experiments.[18−22,35] For the hematite nanorods in sample 2, we only found weak curvature in the χ vs T profile (Figure 3c) and the Morin transition is not apparent. The temperature, T^*, marked in Figure 3c where a minimum appears in the FC/ZFC curves at both 100 and 10 Oe, reflects a magnetic phase transformation in the structure.[36−38] Similar magnetic phase transformations at sufficiently low temperatures have also been found in nanocrystals resulting from surface spin disorder.[36] The existence of disordered surface spins is displayed by the nonsaturation character of the magnetization as shown in Figure 3d. Adatoms or clusters adsorbed on the particle surface will result in disorder of surface spins.[37] At sufficiently low temperature, the exchange interaction in each particle dominates, the surface spins become ordered, and the magnetization increases accordingly.[36−38] From the TEM and FTIR investigations, we know that the hematite nanorods in sample 1 are well-crystallized single crystals with a clean and smooth surface; the nanorods in sample 2 are shorter, with many pores and probably adsorbed phosphate ions on the surface. These factors will likely suppress the Morin transition in sample 2, similar to the situation for spherical nanoparticles. In Morin's experiments in 1950,[17] the magnetic transition did not occur when 1.0% of Ti was added to the pure hematite. By replacing the iron powder starting materials with nickel−iron alloy micrometer particles during the iron−water reaction, we obtained Ni (less than 1%)-doped hematite nanorods. For these Ni-doped samples, we have also observed the absence of a Morin transition, possibly due to the crystalline distortion in the hematite lattice, by analogy to the effect of adding Ti.

Conclusion

The magnetic properties of two types of hematite nanorods prepared by an iron−water vapor reaction and by hydrothermal methods have been studied by SQUID magnetometry from 2 to 200 K. Nanorods prepared by the iron−water vapor reaction, with a diameter of 20−100 nm and a length of 1−2 μm, exhibit an MD-type behavior and have a Morin transition temperature of 122 K. Under a low external field of 10 Oe, a decrease of magnetic susceptibility at 122 K has been observed and is attributed to the possible competition between the 1-D shape anisotropy and the magnetocrystalline anisotropy. The nanorods prepared by hydrothermal methods, with a diameter of 50−60 and 500 nm long, are found to display a PSD-type behavior, and the Morin transition is not in evidence.

Acknowledgment. We thank the EPSRC and the Royal Society (U.K.) for financial support.

CM062375A

(35) Zysler, R. D.; Fiorani, D.; Testa, A. M. *J. Magn. Magn. Mater.* **2001**, *224*, 5−11.
(36) Gao, Y. H.; Bao, Y. P.; Beerman, M.; Yasuhara, A.; Shindo, D.; Krishnan, K. M. *Appl. Phys. Lett.* **2004**, *84*, 3361−3363.
(37) Berkowitz, A. E.; lahut, J. A.; Jacobs, I. S.; Levinson, L. M.; Forester, D. W. *Phys. Rev. Lett.* **1975**, *34*, 594−597.
(38) Kodama, R. H.; Berkowitz, A. E.; McNiff, E. J.; Foner, S. *Phys. Rev. Lett.* **1996**, *77*, 394−397.